# The Analysis of X(3872) with BaBar

Bradley J. Wogsland

August 18, 2007

**Abstract**

Meson states which do not fit into the Charmonium spectrum have recently been discovered at the B-Factories by the BaBar and Belle collaborations. This is a very exciting period for the field as new resonances are discovered every few months. I report on a search for the decay process $B \to X(3872)K$ using $\Upsilon(4S) \to B\overline{B}$ decays collected with the BaBar detector at the PEP-II asymmetric energy B-Factory at the Stanford Linear Accelerator Center (SLAC). In addition I present my involvement the Detector of Internally Reflected Cherenkov Light (DIRC) subsystem as well as installing the Limited Streamer Tubes (LST) subsystem for the BaBar detector.

# 1 Physics Motivation

## 1.1 Mesons Spectroscopy

Quarks were postulated by Murray Gell-Mann and George Zweig to explain the plethora of new states being discovered by high energy colliders in the 1960s [1]. Group theory considerations allow many possibilities of quark combinations (any combination with 3n quarks will do), but only two have been observed in nature. The fermionic combination, called a baryon, combines 3 of the spin 1/2 quarks. The bosonic combination, called a meson, combines a quark and an antiquark. It is the latter combination which is of interest to the current study.

The theory of quarks interactions mediated by the strong force is called Quantum Chromodynamics (QCD). Just like in Quantum Electrodynamic (QED) interactions, in QCD there are conserved quantities: angular momentum, parity, C-parity, and isospin. Only certain quantum numbers are allowed for mesons. The orbital angular momentum L can take on any value, but the spin of the quarks can only be aligned parallel ($\uparrow\uparrow$) or antiparallel ($\uparrow\downarrow$). This means the total angular momentum can take on the values $J = |L - S|, ..., L + S$. Similarly, the parity for mesons takes the value $(-1)^{L+1}$ and C-parity takes the value $(-1)^{L+S}$. Isospin is an expression of the SU(2) symmetry of the particles formed from u and d quarks. For example, the proton and neutron form a doublet so they are assigned $\mathrm{I} = \pm\frac{1}{2}$. Mesons which do not bear these normal quantum numbers are called exotics.

| L | $J^{PC}$ |
|---|---|
| 0 | $0^{-+}$, $1^{--}$ |
| 1 | $1^{+-}$, $0^{++}$, $1^{++}$, $2^{++}$ |
| 2 | $2^{-+}$, $1^{--}$, $2^{--}$, $3^{--}$ |

Table 1: Meson Quantum Numbers

This is, however, a static picture; reality is much more dynamic. In QCD higher order terms of the expansions of interactions do not decrease in magnitude and are therefore not negligible as they are in QED. As it turns out though, in the lower energy regime of BaBar, the static quark model gives fairly good results. Theorists have several different roads to explain the observed spectrum. Phenomenological Models of charmonium use a QED-like 1/r potential plus a string-like potential. In addition they often include several more terms for finer splittings. This yields a potential of the form

$$V(r) = -\frac{4}{3}\frac{\alpha_s}{r} + kr + ... \tag{1}$$

The basic idea is to model the entire spectrum with the fewest parameters. The Lattice QCD approach is a computationally intensive approach beginning with the first principles. Space is divided up into lattice points and quarks

are allowed to evolve according to the laws of QCD. In between these two are Effective Theories which try to take into account the best of both approaches.

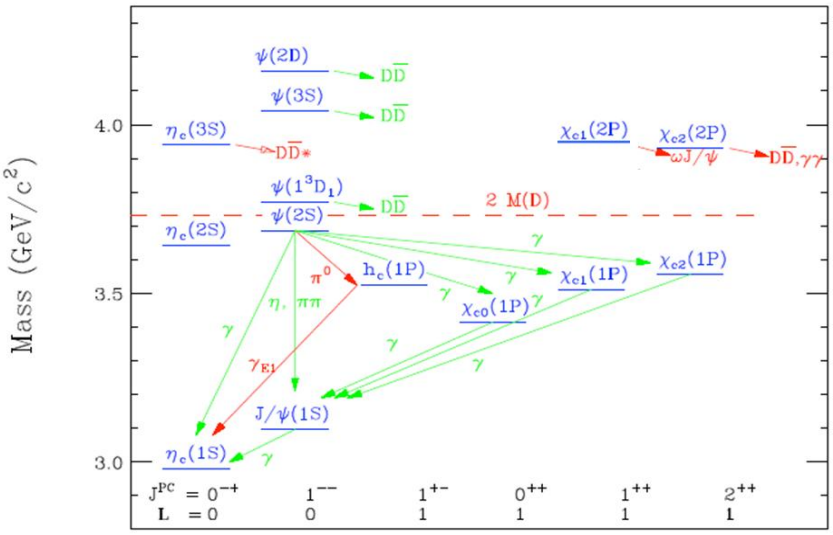


Figure 1: The Charmonium Spectrum

## 1.2 Measuring the Quantum Numbers of the X(3872)

The X(3872) was discovered by Belle in 2003 [2] and subsequently confirmed by CDF [3], DØ [4] and BaBar [5] as a high-mass, narrow-width state decaying into $J/\psi\pi^+\pi^-$. The average of these experiments yields a mass of 3871.2 $\pm$ 0.5 MeV and width <2.3 MeV at the 90% confidence level [6]. The motivation for continued study of this particle is compelling. The X(3872) does not naturally fit into the Charmonium spectrum chown in Figure 1 and numerous theoretical explanations have been proposed. The myriad possibilities include a bound state of $D^*\overline{D}$ very close to the $D_0^*\overline{D}_0$ threshold [7] [8] [9], a hybrid charmonium 5 state [10], a diquark-antidiquark state [11], and a conventional charmonium state [12].

The purpose of the present work is to clarify which theoretical model is correct by measuring the quantum numbers of the X(3872). The straightest route would be to do an angular analysis, but there are not enough events with current statistics so a more indirect route is needed. The isospin (I) of the X(3872) is still unknown, but we can learn much about it just from decay modes. The $J/\psi$ has no isospin, and pions have isospin $I_{\pi^\pm} = \pm 1$ and $I_{\pi^0} = 0$. Because the X(3872) decays into the $J/\psi\pi^+\pi^-$ channel it must have isospin 0

or 1. To characterize it further, we also look at the $J/\psi\pi^0\pi^0$ channel which has I = 0. Decay into this channel would also imply $C = -$. Furthermore, Voloshin has shown that defining the ratio of branching fractions as

$$R = BF(X \to J/\psi\pi^0\pi^0)/BF(X \to J/\psi\pi^+\pi^-) \tag{2}$$

that this number should be 0 or 0.5 depending on whether the isospin of the X(3872) is 1 or 0 [7]. So far Belle has reported R < .78 which does not clarify the isospin [2]. The present work should be able to improve on this figure by a factor of 2 due to an increased dataset. This will determine R and hence the isospin and C-parity of the X(3872).

### 1.3 Particle Production

Particles can be produced directly. For example, BaBar produces the $\Upsilon(4S)$ meson directly from $e^+e^-$ collisions. Fixed target experiments also produce particles directly. In addition, indirect production of particles is also possible. This is when processes occur further down the decay chain. An example of this is the B meson decay which is a major focus of the current work, $B^+ \to X(3872)K^+$, because the B used is itself a decay product of the $\Upsilon(4S)$ created directly by PEP-II. Quantum numbers also restrict states which can be produced.

### 1.4 Detecting Resonances

Short lived particles like mesons are detected as resonances of their decay products by looking in the invariant mass spectrum, where the relativistic 4-momenta of the decay products are added together. To derive a probability function to fit this spectrum to we start with the wave function for an unstable particle and compute the Fourier transform of the decaying particle's wave function into energy space. Taking the inner product we find the probability of a state being found at a given energy,

$$|\psi(E)|^2 = \frac{\hbar^2|\psi(0)|^2}{2\pi(\frac{\Gamma^2}{4} + (E - E_0)^2)} \tag{3}$$

which is the Breit-Wigner functional form. This function is convoluted with a normal Gaussian to account for statistical errors.

## 2 Analysis Strategy

The idea of this analysis is to look for resonances in the decay of $B \to J/\psi\pi\pi K$ where $\pi\pi$ can be either $\pi^+\pi^-$ or $\pi^0\pi^0$ and $K$ can be $K^+$, $K^-$, $K_L$, or $K_S$. The X(3872) was originally discovered in the charged pion channel and has not been observed in the neutral pion channel. I began my analysis as a blinded reconstruction of these decay channels. I establish significant event variables and tried to minimize background in simulated events, or Monte Carlo, before

filtering the data. After that a maximum likelihood analysis will be done using probability density functions (PDFs) for the significant variables. Finally the analysis will be unblinded and I will have either signal or an upper limit for R, the ratio of the neutral and charged pion channel branching fractions described above.

## 2.1 Estimation of Results

The number of $B\overline{B}$ pairs produced for BaBar is given by

$$N_{B\overline{B}} = \sigma\mathcal{L} \tag{4}$$

where $\sigma$ is the interaction cross section and $\mathcal{L}$ is the integrated luminosity. So far BaBar has integrated roughly 500 fb$^{-1}$ of data on a variable cross section of around 1 nb. To calculate the branching fraction we use

$$BF(decay) = \frac{N_S}{N_{B\overline{B}}\epsilon_{detector}\Pi BF(subdecay)} \tag{5}$$

where $N_S$ is the number of signal events, $\epsilon_{detector}$ is the efficiency of the detector and the BF(subdecay) are branching fractions of the subdecays down to the particles actually detected. BaBar's previous branching fraction measurement in the channel $B^+ \to J/\psi\pi^+\pi^-K^+$ saw 61.2 ± 15.3 signal events in 232 million $B\overline{B}$ pairs [13].

The efficiency for detection of a charged particle in BaBar is roughly 90%, and the efficiency for detection of a photon is roughly 80%. The $J/\psi$ reconstruction uses both the electron and muon decay channels representing branching fractions of 5.94 ± .06 % and 5.93 ± .06 % respectively [6]. The $\pi^0$ branching fraction to two photons is 98.798 ± .032 % [6]. $K_S$ reconstruction was done was done from two charged pions which represents a 69.20 ± .05 % branching fraction [6]. The electrons, muons, $\pi^\pm$ and $K^+$ are all detected directly. These estimates are summerized in Table 2.

| Decay Channel | $\epsilon_{detector}$ | $\Pi BF$ | $N_S$ |
|---|---|---|---|
| $B^+ \to XK^+$, $X \to J/\psi\pi^0\pi^0$ | .30 | .116 | 32.7 |
| $B^0 \to XK_S$, $X \to J/\psi\pi^0\pi^0$ | .27 | .0802 | 20.3 |
| $B^+ \to XK^+$, $X \to J/\psi\pi^+\pi^-$ | .59 | .119 | 132 |
| $B^0 \to XK_S$, $X \to J/\psi\pi^+\pi^-$ | .53 | .0821 | 81.7 |

Table 2: Branching fraction corrections and signal event estimates (neutral pion channel estimates assume R = .5)

The significance of these measurements can be estimated with

$$\frac{N_S}{\sqrt{N_S + N_B}} \tag{6}$$

where $N_B$ is the number of background events under the signal. With my estimated 50 signal events in the neutral channels this means a $5\sigma$ measurement is possible even with an equal number of background events. On the other hand, if no signal is observed the current upper bound on the branching fraction can be decreased by a factor of two.

## 2.2 Candidate Reconstruction

Candidate reconstruction parameters are used for signal extraction from the dataset. I determined and tested them using MC data samples and eventually incorporated them into the filter described in the subsequent section.

### 2.2.1 $J/\psi$ Reconstruction

The reconstruction of the $J/\psi$ was done with two differing sets of criteria, one loose and one tight. For electrons detected as a cluster in the EMC, if they fit together geometrically and had an invariant mass in the range 2.5 - 3.3 GeV they were accepted as a $J/\psi$ candidate. For muon pairs reconstructed as charged tracks, if they fit together geometrically and had an invariant mass in the range 2.8 - 3.3 GeV they were accepted as a $J/\psi$ candidate. The lower energy cut on the $e^+e^-$ channel is used because they are more susceptible to energy loss. Similarly, the tight $J/\psi$ reconstruction looks in both decay channels, but adding a PID requirement on the electrons and muons.

### 2.2.2 Photon Reconstruction

The photon selection criteria are formed from energy deposition in the EMC unpaired to a charged track. This lab energy of the photon is required to fall in the range .03 - 10 GeV. Additionally, the lateral momentum of the particle must fall in the range 0 - .8.

### 2.2.3 $\pi^0$ Reconstruction

The $\pi^0$s were reconstructed using two photons as defined in the previous section. The only additional requirement was that the two photons had an invariant mass in the range 100 - 170 MeV.

### 2.2.4 $\pi^\pm$ Reconstruction

The $\pi^\pm$ mesons were reconstructed by looking for a charged particle track through the detector which is identifiable as such. No PID requirement is applied.

### 2.2.5 $K^\pm$ Reconstruction

The $K^\pm$ reconstruction was done with a charged track whose mass is too large to pass the pion PID test.

### 2.2.6 $K^0$ Reconstruction

$K_S$ reconstruction was done was done from two charged pions. Only particles with masses in the range 472.67-522.67 MeV are accepted. The $K_L$ reconstruction, however, remains to be implemented.

### 2.2.7 $B$ Reconstruction

The reconstruction of the B meson differs for each of the channels involved based on the particles used in those channels. For the $B^+ \to J/\psi\pi^+\pi^-K^+$ channel the tight definition of $J/\psi$ is used in combination with the $\pi^\pm$ and $K^+$ as defined above. The Add4 algorithm then justs adds the 4-momenta of the particles to produce the $B$ at the interaction point. Then $m_{ES}$ is required to fall in the range 5.1 - 5.3 GeV and $\Delta E$ in between $\pm$ 0.3 GeV. For the $B^+ \to J/\psi\pi^0\pi^0K^+$ channel the tight definition of $J/\psi$ is used in combination with the $\pi^0$ and $K^+$ as defined above, but dropping the requirement that the $K^+$ fails the pion PID test. A tree-fitting algorithm fits particles at each level of the decay chain all the way up to the $B$ while constraining the particle masses and beam energy to their nominal values. Finally $m_{ES}$ is required to fall in the range 5.2 - 5.3 GeV and $\Delta E$ in between $\pm$ 0.3 GeV. For the $B^0 \to J/\psi\pi^+\pi^-K_S$ channel the tight definition of $J/\psi$ is used in combination with the $\pi^\pm$ and $K_S$ as defined above. The Add4 algorithm is again used and then $m_{ES}$ is required to fall in the range 5.1 - 5.3 GeV and $\Delta E$ in between $\pm$ 0.3 GeV. For the $B^0 \to J/\psi\pi^0\pi^0K_S$ channel the tight definition of $J/\psi$ is used in combination with the $\pi^0$ and $K_S$ as defined above. The Add4 algorithm then used without constraining the $B$ to the interaction point. Finally $m_{ES}$ is required to fall in the range 5.1 - 5.3 GeV and $\Delta E$ in between $\pm$ 0.3 GeV.

## 2.3 Filter Design

A filter was written to go through the data and pull out events that fall into the several decay channels chosen for this analysis using the reconstruction modes described above. Simulated data or Monte Carlo (MC) of the several decay channels was looked into and the filter efficiency was found to be in the range 52-54%. Comparing this to the estimates this is roughly what was expected for the charge pion channels but significantly better than expected for neutral pion channels. However, when looking at generic B $\to J/\psi + anything$ MC the filter eliminates only about half, meaning the filtered data will still contain a significant portion of background.

NTuples were first created from reconstructed MC data to contain information on the particles and their interactions with the detector. Then generator level Ntuples were made with the same MC data to elucidate the effect of the detector.

## 2.4 Monte Carlo

Monte Carlo for each of the several channels incorporated in the study were produced. These are listed in Table 3. The $\psi(2S)$ channels were included for comparison. In addition, generic decays of charged and neutral B mesons were also used in this study. This MC is used to estimate the efficiency of detecting the particles of the decay chain $\epsilon_{detector}$. In addition, MC can be used to identify and eliminate background while holding on to signal events. Background comes from two main sources: (1) continuum events, that is $e^+e^- \rightarrow q\bar{q}$ where the quark-antiquark pair can be u, d, s or c, and (2) other B-decays.

| Decay Channel | Events |
|---|---|
| generic $B^+B^-$ decays | 542226433 |
| generic $B^0B^0$ decays | 546502225 |
| $B^+ \rightarrow X(3872)K^+$, $X(3872) \rightarrow J/\psi\pi^0\pi^0$ | 117000 |
| $B^0 \rightarrow X(3872)K_S$, $X(3872) \rightarrow J/\psi\pi^0\pi^0$ | 117000 |
| $B^+ \rightarrow \psi(2S)K^+$, $\psi(2S) \rightarrow J/\psi\pi^+\pi^-$ | 117000 |
| $B^+ \rightarrow \psi(2S)K^+$, $\psi(2S) \rightarrow J/\psi\pi^0\pi^0$ | 117000 |
| $B^+ \rightarrow X(3872)K^+$, $X(3872) \rightarrow J/\psi\pi^+\pi^-$ | 117000 |
| $B^+ \rightarrow X(3872)K^+$, $X(3872) \rightarrow J/\psi\rho^0$, $\rho^0 \rightarrow \pi^0\pi^0$ | 117000 |
| $B^0 \rightarrow \psi(2S)K_S$, $\psi(2S) \rightarrow J/\psi\pi^+\pi^-$ | 116000 |
| $B^0 \rightarrow \psi(2S)K_S$, $\psi(2S) \rightarrow J/\psi\pi^0\pi^0$ | 117000 |
| $B^0 \rightarrow X(3872)K_S$, $X(3872) \rightarrow J/\psi\pi^+\pi^-$ | 117000 |
| $B^0 \rightarrow X(3872)K_S$, $X(3872) \rightarrow J/\psi\rho^0$, $\rho^0 \rightarrow \pi^0\pi^0$ | 117000 |

Table 3: Available MC sets

## 2.5 Data Sample

The BaBar data sample includes almost 500 million $B\overline{B}$ decays, however, the BaBar collaboration produces general purposes skims of the data. This considerably lowers the number of events to be filtered as can be seen in Table 4, where the data reduction of the JpsitollTight skim which is used in this analysis is shown. This skim uses the tight definition of a $J/\psi$ decaying to two leptons described below. Any events with a $J/\psi$ fitting this definition are included in the skim.

## 2.6 Discriminating Variables

In this section the variables used for the event selection are outlined. Some of the discriminating variables available include kinematic variables specific to B decay, thrust angles, Zernicke moments [14], and Fox-Wolfram moments [15]. We will produce distributions of the variables on data and MC. The agreement between data and MC in terms of normalization and/or shape will be studied.

| Dataset | Total Events | Skimmed Events |
|---|---|---|
| Run 1 | 294526570 | 1724770 |
| Run 2 | 944926749 | 5077127 |
| Run 3 | 471014621 | 2767461 |
| Run 4 | 1581717366 | 8855435 |
| Generic MC | 1124768000 | 5640094 |

Table 4: JpsitollTight skim events per Run with simulated events for comparison

### 2.6.1 B Decay Kinematic Variables

In order to separate true B mesons that are produced in $e^+e^- \rightarrow B\overline{B}$ from background the following two kinematic variables of the reconstructed B meson are used:

$$\Delta E = E_B^* - \frac{\sqrt{s}}{2} \tag{7}$$

$$m_{ES} = \sqrt{\frac{(\frac{s}{2} + \mathbf{p}_i \cdot \mathbf{p}_B)^2}{E_i^2} - \mathbf{p}_B^2} \tag{8}$$

where $E_i = E_{e^+} + E_{e^-}$ and $\mathbf{p}_i = \mathbf{p}_{e^+} + \mathbf{p}_{e^-}$ are the total energy and momentum of the $e^+e^-$ system, $s = E_i^2 - \mathbf{p}_i^2$ is the center of mass energy squared, $E_B^*$ is the energy of the reconstructed B meson in the $e^+e^-$-rest frame and $\mathbf{p}_B$ is the 3-momentum of the B meson in the lab frame. For a true B meson we expect $\Delta E$ to peak at zero. The energy substituted mass, $m_{ES}$, should also peak at the value of the B mass around 5.279 GeV/$c^2$ . Because of the detector resolution, $\Delta E$ and $m_{ES}$ represent an almost uncorrelated pair of variables in the two dimensional space of momentum and energy.

The requirement that the 4-momentum of the reconstructed B meson should match the four-momentum of a B which comes from $e^+e^- \rightarrow B\overline{B}$ with well known initial energy and momentum can also be used.

## 2.7 Work in Progress

### 2.7.1 Optimization

Optimization is done to maximize the number of signal events relative to the background. The reconstruction cuts must be optimized for each of the particles in the decay chain, namely $B^{\pm}$, $J/\psi$, $\pi^{\pm}$, $K^{\pm}$. The resonant signal will eventually be based on one or more of $m(J/\psi\pi\pi)$, $\Delta E$ and $m_{ES}$.

### 2.7.2 Data/MC Comparison

So far only filter and skim rates have been compared but eventually the MC will be used to establish which kinds of backgrounds are present and can be

eliminated. These backgrounds usually include mainly continuum events and other B-decays.

### 2.7.3 PID Corrections

The current reconstruction used in the filter ignores some PID information which we may need to take into account later in the analysis. For example it may be profitable to use a PID requirement from the DIRC on the charged pions as well as kaons.

One of the difficulties in the reconstruction of the neutral pion channels is the combinatorial problem of matching the correct photons to the correct pions while not including any photons which may be produced in the decay of the other B meson. I am developing a neural net program to optimize the correct selection of photons to eliminate the misidentifications.

### 2.7.4 Tracking Corrections

As part of the fine-tuning of the analysis, selected events will be examined to see if any tracking corrections are required, for example by fitting the decay chain with a tree-fitting algorithm rather than Add4.

### 2.7.5 Efficiency Corrections and Systematic Errors

The number of $B\overline{B}$ events will be verified and the secondary branching ratios will be checked. The efficiency of the fit will be calculated and the fit itself validated. As mentioned earlier, filtering of the MC has shown that efficiencies for the neutral pion channels are significantly higher than expected. However, my studies of the pion reconstruction have shown that this is do to at least partially to misidentification of photons.

### 2.7.6 Inclusion of Runs 5 and 6 in the Dataset

The run 5 dataset is complete and skimmed. It needs only to be filtered before inclusion into the analysis. Run 6 is still underway however, but skimming is proceeding concurrently so it should be available later this year.

### 2.7.7 Invariant $J/\psi\pi\pi$ Mass Spectrum

We will look for this as a resonant structure in the invariant $J/\psi\pi\pi$ mass. The X(3872) peaking region is currently blinded to avoid biasing the results. When the data is finally unblinded a maximum likelihood analysis will be done on the peak. The results of this analysis will include branching ratios for the various channels, the mass & natural width (lifetime) of the X(3872), and limits in the $\Delta m - R$ plane. With the statistics available we should be able to establish the isospin and C-parity of the X(3872). This will take us much closer to understanding what exactly the X(3872) is.

#### 2.7.8 Expanding the Scope

As with any venture into uncharted territory one cannot be sure the exact direction exploration will take. With the level of statistics available other new resonances may be seen elsewhere in the spectrum which would also need to be analyzed. For example, previous analysis has seen evidence for the Y(4260) in the charged pion channel but did not have enough events to confirm it. In addition, other channels like $B^0 \to X(3872)K_L$ will need to be included. If R = .5 and $I_{X(3872)} = 1$, then there is a good change that it is part of a triplet rather than a singlet. In this case there would be charged partners visible in the $J/\psi\pi^0\pi^\pm$ invariant mass spectra. To date these have not been observed, but still cannot be rule out. There are a myriad of possible directions into which this analysis might be expanded.

# 3 The BaBar Detector

## 3.1 The Dataset

In the early 1990's it was realized that a high statistics detector at energies significantly lower than the current energy frontier could nevertheless make significant contributions to high energy physics. Most importantly, a detector running at the $\Upsilon(4S)$ resonance would produce pairs of $B$ mesons, allowing for the study of CP violation in $B$ decays as it had earlier been studied in kaons.

## 3.2 Detector Overview

Figure 2 is a cutaway view into the BaBar detector. The 3.1 GeV positrons collide with 9 GeV electrons at the center of the interaction region creating an $\Upsilon(4S)$. The resulting boost lengthens $B$ meson lifetimes in the lab frame. Charged particle tracks are measured by a five layer double-sided Silicon Vertex Tracker (SVT) and a 40 layer Drift Chamber (DCH) located within a 1.5T axial magnetic field. Charged hadrons are identified by combining energy loss information from tracking (dE/dx) in the DCH with the measurements from Detector of Internally Reflected Cherenkov Light (DIRC). The CsI(Tl) crystal Electromagnetic Calorimeter (EMC) measures the energies of photons and electrons. The magnetic flux is returned via an iron superstructure which is instrumented with Resistive Plate chambers (RPCs) and Limited Streamer Tubes (LSTs) for muon and neutral hadron identification. A more detailed description can be found in [16].

## 3.3 The DIRC

#### 3.3.1 Cherenkov Radiation

Although there is a fundamental speedlimit for particles traveling in a vacuum, particles can travel faster than the speed of light in matter. When passing

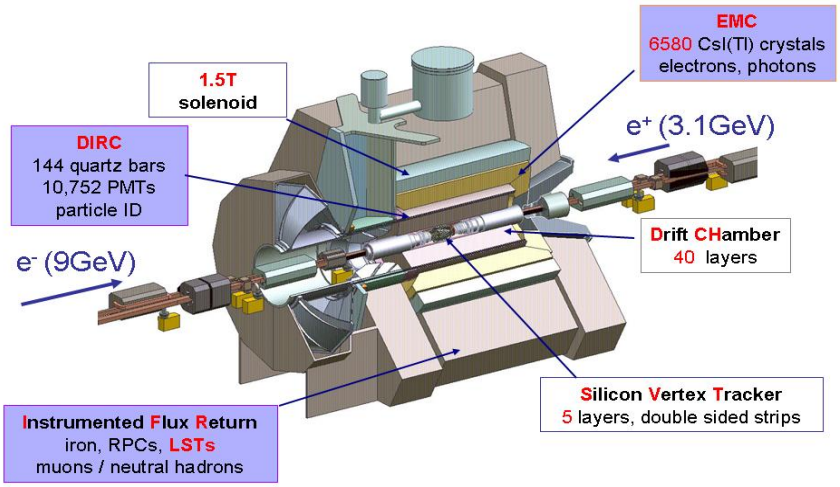


Figure 2: A cutaway view of the BaBar detector.

through a transparent medium at a superluminal velocity a particle will emit Cherenkov light. The angle away from the particle's path with which that light will be emitted is

$$cos\theta_C = \frac{1}{\beta n(\lambda)} \tag{9}$$

where $\theta_C$ is the angle, $\beta$ is the velocity of the particle relative to the speed of light in a vacuum ($\beta$ = v/c), and n is the index of refraction of the medium through which the particle is passing which is a function of the wavelength $\lambda$. Recalling the relativistic relations $\beta = p/E$ and $E = \sqrt{p^2 + m^2}$ then we get

$$m = p\sqrt{n^2 cos^2\theta_C - 1}. \tag{10}$$

which is solved for the mass since the DCH measures momentum.

### 3.3.2 Overview of the DIRC Design

The main purpose of the Detector of Internally reflected Cherenkov Light (DIRC) is to provide $\pi$-K separation up to momenta of 4.2 GeV/c, which is the highest momentum for those particles decaying from $B$s in BaBar [17]. A measurement of $\theta_C$ versus p is shown in Figure 3. This is done by measuring the Cherenkov angle $\theta_C$ to get the $\beta$ of a particle as described in Equation (10).

Figure 4 is a cross-section of the DIRC. Cherenkov photons are produced when a particle passes through the quartz bars which then direct the photons

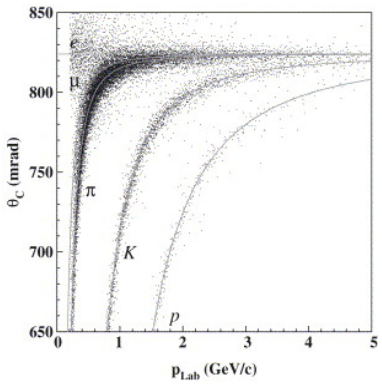


Figure 3: Cherenkov angle vs. momentum as measured by the DIRC.

down toward the photomultiplier tubes (PMTs). Passing out of the quartz wedge into the water of the Stand-Off Box (SOB) the light travels to the PMT were it is detected and recorded.

Quartz was chosen as the Cherenkov radiator because its index of refraction n = 1.458 is just above that required to undergo total internal reflection of the Cherenkov light from particles incident at 90 degrees, thus allowing it to serve as a lightguide as well. In addition, quartz can be polished to allow for very little light loss. Several kinds of quartz were tested, but in the final analysis fused silica was chosen because of it's radiation hardness [18]. A study of the background [19] was also done and shown to be significantly less than that produced in the SOB. The quartz bars are protected inside watertight barboxes which each hold 12 bars. A nitrogen atmosphere is flowed through the barboxes to keep them dry because water condensation would break the total internal reflection. The gas flow, temperature and humidity in the barboxes are all monitored regularly. 12 of these barboxes are coupled to quartz wedges which are connected to the SOB.

The SOB contains ultrapure deionized water which provides the optical coupling between the quartz bars and the PMTs. Water at n = 1.33 is very close to this value and so it can break the internal reflection for most photons produced and provides for an amplification of the opening angle by $\frac{n_{quartz}}{n_{water}} = 1.096$. $H_2O$ is one of the best solvents in existence, however, and in its natural state usually has a reasonably large concentration of dissolved ions. The deionized water inside the SOB is looking to its surroundings to provide these ions. The water is circulated through the SOB roughly once every day and deionized, irradiated with UV light to kill bacteria, and kept under nitrogen. Constant monitoring of the water level, pH value, temperature, inflow and outflow rates insures proper functioning.

BaBar chose to use PMTs to detect the photons because they are well developed, efficient and inexpensive compared to alternatives. We used ETL 9125FLB17 PMTs because of a lack of corrosion and transmission loss observed

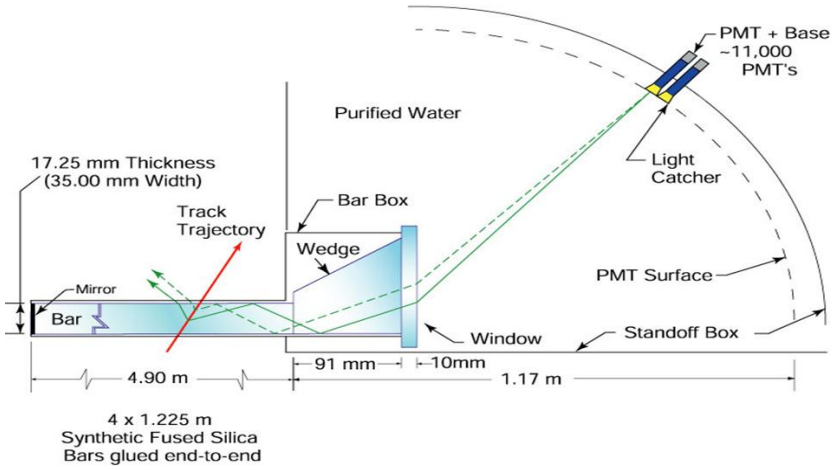


Figure 4: A schematic cross-section of the DIRC.

with these PMTs during testing. It is a cylindrical PMT with a diameter of 28.2 mm, the surface of which is 85% active photocathode. The remaining dangers for these PMTs are helium, which can pass through the surface and break the vacuum, and magnetic fields, which can alter the particle trajectories inside the PMT [20]. Helium is not used anywhere in the detector, but is used by our PEP-II colleagues when leak-checking the accelerator. We protect the backside of the PMTs whenever He is used nearby. The 1.5 T magnetic field produced inside the detector is blocked from the PMTs by an active bucking coil and a magnetic shield down to the level of a few gauss. Between the PMTs are rhodium reflectors [21] designed to reflect light into the PMTs, leading to the effective active surface area for light collection to be 90%. We calibrate the PMTs every few days with a LED light source. The average timing resolution measured by the PMTs is $\sigma_t = 1.5$ ns, which allows for background elimination.

The main sources of uncertainty in the $\theta_C$ measurement are our ignorance about the color of emitted photons and the geometrical uncertainties about where the light exited the quartz bar's surface and on the surface of a PMT the photon landed. This total uncertainty from these sources is $\sigma_\theta = 9.6$ mrad.

The photon yield has been found to be falling over time by around 3% per annum for reasons not well understood. This photon loss was studied using dimuon events. Only .3% of this drop is due to failed PMTs, which expire at a rate of around 30 a year. Only 190 of 10,752 PMTs have failed over the life of the experiment. There seems to be a correlation between the photon loss with

the performance of BaBar's Drift Chamber, which identifies charged tracks for the DIRC [22]. Nevertheless, the rate of loss is small enough not to be an issue during the lifespan of the experiment.

The DIRC electronics are mainly responsible for powering and collecting data from the PMTs [23]. Six CAEN HV crates power the HV on the 10,752 PMTs. The signals from the photons detected by these PMTs are in turn read out in 12 WieNeR crates attached to the outside of the SOB. Inside each WieNeR crate are 14 DIRC Frontend Boards (DFBs) and a DIRC Crate Controller (DCC) board. Since the WieNeR crates are inside the the DIRC's magnetic shield they are each cooled by 6 crate fans and an external chiller.

### 3.3.3 Operational Issues

I served as DIRC commissioner from June 2006 - June 2007 when I was responsible for the day-to-day operations of this subsystem.

**Fall 2006 Dust Problems** During the fall 2006 BaBar shutdown the DIRC experienced a string of failures in many of the electronics. It was determined to be due to the humidity and dust from a nearby construction site present in the hall as a result of the concrete radiation shielding as well as the DIRC magnetic shield being removed for the LST installation. The DIRC electronics were shut off 5 in mid-August while the gas and water systems, however, were kept running. In late September the DIRC HV and readout electronics were turned back on to do some online calibration testing. Simultaneously the WieNeR crates, which had hitherto been run in test mode, were switched to normal mode. In test mode none of the crates failsafe mechanisms are running and one must rely on EPICS to shut off the crate if there is a problem. In normal mode the crate's internal logic can shut it down if a failure is detected. The dust and moisture accumulation short circuited and corroded the DFBs, DCCs and WieNeR crate internal electronics. It was decided to completely shutdown the DIRC electronics until the concrete shielding again blocked out the dust and humidity and to repair the damaged boards while preventatively treating all the rest.

Drastic remediation was required to restore the functionality of the DIRC and prevent further problems. As commissioner I was significantly involved in this process. We removed 180 readout circuit boards were removed from the detector. Each board also had a protective metal plate which was removed and then the boards were thoroughly cleaned. Then a conformal coating was applied to seal the boards against future corrosion problems. Several of the WieNeR crates also required internal repairs due to faulty power supplies and/or CAN-BUS readout problems. Once these repairs had taken place all the crates were cleaned and new filters were added to the air intakes to block any future dust. Then all the boards were tested before putting them back into the detector. To monitor conditions inside the magnetic shield we placed humidity sensors (described in the LST section) directly on the crates.

**May 2007 Accelerator Coolant Leak** On May $1^{st}$ one of the accelerator magnets failed to turn off during a shutdown procedure while its coolant system did, causing a fire and steam which burst the water coolant lines. Several liters of

water leaked into the detector from this water line. The accident leaked water into the DIRC tunnel, but it traveled down the tunnel to the backward end without going into the barboxes were the quartz bars are stored. The WieNeR crates did not get wet, nor did the back ends of the PMTs. However, higher humidity levels were measured in sectors 5, 6 and 7 so nitrogen flow through the barboxes was increased. Water continued dripping from the DIRC until May 3, when humidity levels in sectors 5, 6 and 7 started to go down as well. The WieNeR crates were powered back up and data was successfully taken with cosmic rays. The accelerator repair took about two weeks and the humidity levels were back down to their normal ranges when data-taking started again.

## 3.4 The EMC

BaBar's Electromagnetic Calorimeter (EMC) is the subsystem for detecting electrons and photons and consists of 6580 CsI(Tl) crystals [16]. It is designed to have an energy resolution of 1% for low energy photons down to 20 MeV, and high energy electrons produced in Bhabha events around 9 GeV. Furthermore, the pixelization of the detector is determined by the need to distinguish the two photons in $\pi^0$ decay. The mass of a $\pi^0$ is calculated by

$$m_{\pi^0} = 2\sqrt{E_1 E_2} sin\frac{\alpha}{2} \tag{11}$$

where $E_1$ and $E_2$ are the energies of the two photons detected and $\alpha$ is the angle between them. The need to detect pions up to 5 GeV requires a resolution of a few mrad.

When one of those particles enters a crystal of the EMC it results in an electromagnetic cascade which deposits energy spread over many adjacent crystals (known as a cluster). More than one local energy maximum (a bump) within a cluster can arise due to the decay of a high energy neutral pion into two photons. We then look for crystals with an energy deposit E > 10 MeV and then add to it crystals with E > 1 MeV that are adjacent to existing cluster member crystals with E > 3 MeV. Good clusters are those which have a total energy E > 20 MeV. A cluster is associated with a charged particle track if its bump location matches a known particle trajectory. If no matching trajectory exists then the cluster likely belongs to a neutral particle like a photon or $\pi^0$.

## 3.5 Installation of the LSTs

### 3.5.1 Iarocci Tubes

Iarocci tubes are basically single wire drift chambers often used in the outer layers of large detectors to detect muons. There is a single central wire held at high voltage in a tube of gas which will cause a detectable avalanche toward the wire when a particle passes through the chamber. The tubes are usually run in streamer mode, which allows for a wide and noiseless HV efficiency plateau for wire diameters in the range 40-220 $\mu$m and tube diameters in the mm to cm range. These detectors are especially useful for detecting muons.

### 3.5.2 LST Subsystem Design

The BaBar collaboration initially chose to use RPCs for $\mu^{\pm}$ and neutral hadron detection, however when these began to fail LSTs were designed to replace them. I was involved in the installation of this new subsystem during the summer and fall of 2006. BaBar's LST system is unique in allowing for a three dimensional measurement in cylindrical coordinates (r,$\phi$,z).

BaBar's Iarocci tubes are 17mm wide, 15mm high and 380mm long and built into submodules containing seven or eight tubes. These tubes are constructed from two submodular-size pieces which are painted with a water-based graphite paint on the inside and then glued together. This inner wall paint is held at ground to create a voltage with the gold plated anode wire in the center of each tube at around 5500V. Inside the tubes is a gas mixture of 89% $CO_2$, 3% argon and 8% isobutane which is not flammable and has good quenching properties. This gas is cycled through at a rate of 2.5 l/min which corresponds to replacing the entire gas volume in the LSTs about once per day. The barrel system of BaBar is sextant shaped and consists of 19 layers, all of which were originally equipped with RPCs. However, only the inner 18 layers are accessible for the LST installation. To offset the loss of absorbing material between layers 1 and 19, brass was interlaced with LST modules every other layer beginning with layer 5. When a charged particle passes through a tube, the gas mixture is ionized and a streamer builds up toward the wire. When this signal is read out its layer gives an measurement of r and knowing which tube it is in that layer yields the $\phi$ measurement.

The z-planes used in conjunction with the tubes are 4m long and up to 3.8m wide, depending on which layer they are in. Each plane consists of 96 35mm wide copper strips running longways and glued on a copper ground plate. Two or three submodules are combined with a z-plane to form a complete LST module. When a signal forms in the the tube a signal will also be induced on the z-plane to give the final coordinate of the three dimensional measurement.

### 3.5.3 2006 Installation

The first two sextants of the barrel were installed in 2004 and performed well in the detector, so the other four sextants were scheduled for installation during the four month shutdown in the fall of 2006. To prepare and test the LSTs before installation they were set up in an experimental hall nearby where they could be bombarded by cosmic ray muons from outer space. I was involved in taking plateau curve measurements on each of the LST modules to make sure the gas flow and voltage settings were such that the detector was running in the middle of the streamer region (Figure 5). The curves were produced by counting the number of hits at a given voltage over a 100 second period. At lower voltages the number of counts is proportional to the voltage, but in the streamer region this voltage dependence disappears. Running the detector in the streamer region allows for a high signal to noise ratio. Beyond the streamer region the number of counts takes off again. If an LST chamber did not have

a good streamer region the gas flow was increased, which usually solved the problem.

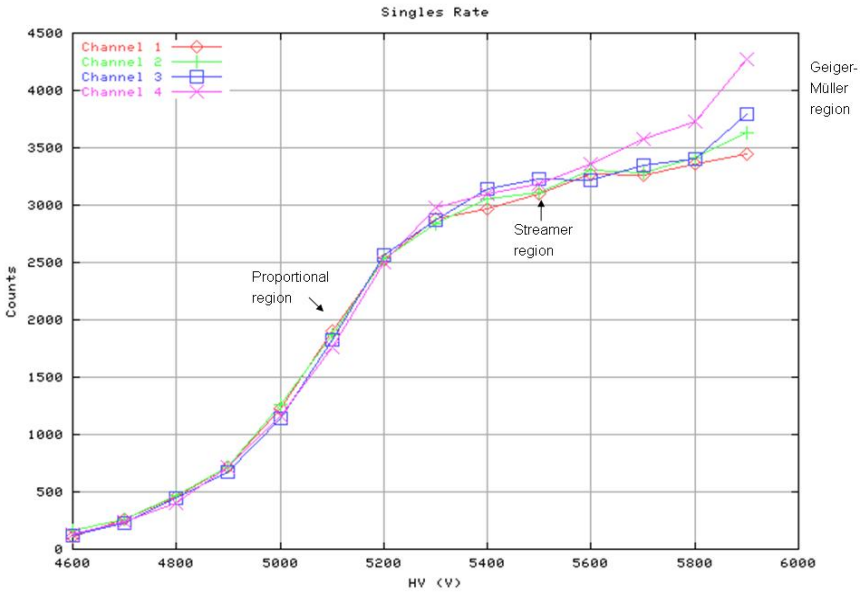


Figure 5: A set of plateau curves for an LST section.

To prevent a HV failure from taking out a large portion of the LST subsystem, each LST module was powered by its own HV line. Thus, several hundred lines had to be fit into the detector to the IFR. I was involved in preparing and running these HV cables. Humidity can be problem for the running of the LSTs by causing sparking of the HV. To prevent this, dry air lines were run into the layers of the IFR and temperature and humidity sensors were placed every few layers to monitor conditions. I built this monitoring system. The sensors used were model Honeywell HIH-3602-A which had six pins: ground, casing, power in, power out, temperature thermistor, and humidity sensor (Figure 6). The sensors had to be handled while grounded, because they were very sensitive to electrostatic discharge. These sensors were then wired to general monitoring boards (GMBs) which were controlled by BaBar's EPICS. In EPICS the raw voltages were converted to meaningful values and the humidity reading was corrected relative to the temperature. We also created a panel to display the temperature and humidity values in the various detector layers and integrated it into displays available in the control room.

### 3.5.4 LST Performance

The barrel muon efficiency was restored in Run 6 by the LSTs from <50% to >90% for muons with energies between 1 and 5 GeV. The subsystem has worked

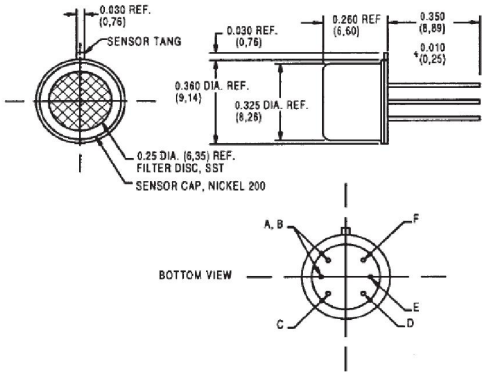


Figure 6: A schematic diagram of the Honeywell HIH-3602-A humidity sensor. The labeled pins are as follows: A, B = thermistor, C = DC voltage supply (5V), D = ground, E = DC voltage out, and F = casing.

very well so far with only minor operational issues. The ability to reconstruct muons is especially important to analyses like mine which include a particle like the $J/\psi$ that is reconstructed from them as described below. In addition, three fourths of BaBar's 100+ citation papers have included the reconstruction of a $K_L$.

# 4 Summary & Outlook

I did work at SLAC commissioning the DIRC and installing the LSTs during 2006-2007. The analysis of the X(3872) is ongoing and will determine that state's quantum numbers. It's scope will be expanding depending on how it develops. In the end a BaBar publication submittable to a major peer-reviewed journal will be produced. This work should be completed by the end of 2008.

# References

[1] M. Gell-Mann, Phys. Letters **8**, 214 (1963).

[2] S. K. Choi et al., Phys. Rev. Lett. **91**, 262001 (2003).

[3] D. Acosta et al., Phys. Rev. Lett. **93**, 072001 (2004).

[4] V. M. Abazov et al., Phys. Rev. Lett. **93**, 162002 (2004).

[5] B. Aubert et al., Phys. Rev. **D71**, 071103 (2005).

[6] W. M. Yao et al., J. Phys. **G33**, 1 (2006).

[7] M. B. Voloshin, Phys. Lett. **B579**, 316 (2004).

[8] N. A. Tornqvist, Phys. Lett. **B590**, 209 (2004).

[9] F. E. Close and P. R. Page, Phys. Lett. **B578**, 119 (2004).

[10] F. E. Close and S. Godfrey, Phys. Lett. **B574**, 210 (2003).

[11] L. Maiani, F. Piccinini, A. D. Polosa, and V. Riquer, Phys. Rev. **D71**, 014028 (2005).

[12] T. Barnes and S. Godfrey, Phys. Rev. **D69**, 054008 (2004).

[13] B. Aubert et al., Phys. Rev. **D73**, 011101 (2006).

[14] F. Zernicke, Physica **1**, 689 (1934).

[15] G. C. Fox and S. Wolfram, Phys. Rev. Lett. **41**, 1581 (1978).

[16] B. Aubert et al., Nucl. Instrum. Meth. **A479**, 1 (2002).

[17] I. Adam et al., Nucl. Instrum. Meth. **A538**, 281 (2005).

[18] J. Cohen-Tanugi et al., Nucl. Instrum. Meth. **A515**, 680 (2003).

[19] A. Yarritu, S. Spanier, and J. Va'vra, IEEE Trans. Nucl. Sci. **49**, 1704 (2002).

[20] P. Bourgeois, M. Karolak, and G. Vasseur, Nucl. Instrum. Meth. **A442**, 105 (2000).

[21] M. Benkebil, R. Cizeron, S. Plaszczynski, M. H. Schune, and G. Wormser, Nucl. Instrum. Meth. **A442**, 364 (2000).

[22] R. Andreasson, (2006), BAD 1637.

[23] P. Bailly et al., IEEE Trans. Nucl. Sci. **47**, 2106 (2000).